Robust and flexible electrochemical lactate sensors for sweat analysis based on nanozyme-enhanced electrode

Li, Pei; Kalambate, Pramod K.; Harris, Kenneth D.; Jemere, Abebaw B.; Tang, Xiaowu (Shirley)

Publisher's version / Version de l'éditeur:
https://doi.org/10.1016/j.biosx.2024.100455
Biosensors and Bioelectronics: X, 17, C, 2024-02-15

Biosensors and Bioelectronics: X 17 (2024) 100455

Contents lists available at ScienceDirect

Biosensors and Bioelectronics: X

journal homepage: www.journals.elsevier.com/biosensors-and-bioelectronics-x

Robust and flexible electrochemical lactate sensors for sweat analysis based on nanozyme-enhanced electrode

Pei Li [a], Pramod K. Kalambate [a], Kenneth D. Harris [b], Abebaw B. Jemere [b,**], Xiaowu (Shirley) Tang [a,*]

[a] Department of Chemistry & Waterloo Institute for Nanotechnology, University of Waterloo, Waterloo, Ontario, Canada
[b] National Research Council Canada, Nanotechnology Research Centre, Edmonton, Alberta, Canada

ARTICLE INFO

Keywords:
Lactate sensor
Electrochemical sensor
Sweat sample
Nanozyme
NiO
Glancing angle deposition (GLAD)

ABSTRACT

In this work, nickel oxide (NiO) nanostructures deposited by glancing angle deposition (GLAD) are fabricated to achieve highly specific catalytic electrooxidation of lactate, replacing the natural enzyme lactate oxidase for electrochemical detection of lactate in sweat. GLAD NiO electrodes exhibit high sensitivity (412 μA mM^{-1} cm^{-2}), wide linear detection range (1–45 mM), low detection limit (3 μM), and excellent specificity in artificial sweat samples. The unique microporous structure of the GLAD NiO electrodes, combined with their high surface area, high catalytic activity, and excellent conductivity, enhance the performance of the sensor and demonstrate their exceptional effectiveness in the sensitive detection of lactate. In-house fabricated gold counter, and stable solid-state Ag/AgCl reference electrodes, all fabricated on a flexible PET substrate along with the GLAD NiO working electrode, demonstrate performance comparable to commercial Pt auxiliary and Ag/AgCl (1M KCl) reference electrodes in lactate detection, along with outstanding flexibility, tested at various radii of curvature (15 mm, 7.5 mm, and 5 mm). The durable and long-lasting GLAD NiO electrode chips overcome numerous challenges in transport, storage, and operation, paving the way for the development of wearable lactate sensors that can detect lactate levels in sweat.

1. Introduction

Lactate is a key metabolite in humans, best known as a waste product generated during intense physical activity. In muscle tissue, lactate tends to be generated under oxygen-poor conditions, and once generated, it is known to reduce muscle output. Thus, it is regularly tracked to assess an athlete's performance and inform training decisions. Moreover, lactate levels can also act as a signal for several pathological conditions (Md Shakhih et al., 2021; Rassaei et al., 2014; Rattu et al., 2020). Imbalance between lactate production and clearance is caused by liver disease, systemic disorders, renal failure, and tissue hypoxia (Kruse et al., 1987; Rassaei et al., 2014; Rimachi et al., 2012). Therefore, changes in blood lactate concentration are currently used to monitor both lactic acidosis as well as endurance in elite athletes using laboratory equipment such as gas chromatography and high-performance liquid chromatography-mass spectrometry (Chuang et al., 2009; Messonnier et al., 2013). A commercial enzymatic lactate monitoring device has also been introduced by Nova Biomedical. Although this sensor provides quick and reliable results, it is based on a perishable enzyme that has limited storage life, and it also requires an invasive sample collection method to draw blood. Recent studies have shown that, in addition to blood lactate, there is also a correlation between exercise intensity and lactate levels in human sweat (Messonnier et al., 2013). As a result, the development of nonenzymatic lactate sensors for sweat sampling has gained significant attention due to the increasing demand for noninvasive and real-time monitoring of lactate levels in both sports performance and healthcare applications.

Electrochemical sensors convey analytical information resulting from the interaction between receptor and analyte, generally with an electrical read-out. These sensors offer numerous advantages, such as low detection limits, rapid response, and cost-effectiveness in terms of equipment (Baranwal et al., 2022; Ronkainen et al., 2010). Enzymes are primarily used as receptor elements due to their high biocatalytic activity and specificity, however, they tend to have certain limitations,

* Corresponding author.
** Corresponding author.
E-mail addresses: abebaw.jemere@nrc-cnrc.gc.ca (A.B. Jemere), tangxw@uwaterloo.ca (X.(S. Tang).

https://doi.org/10.1016/j.biosx.2024.100455
Received 3 January 2024; Received in revised form 6 February 2024; Accepted 10 February 2024
Available online 15 February 2024

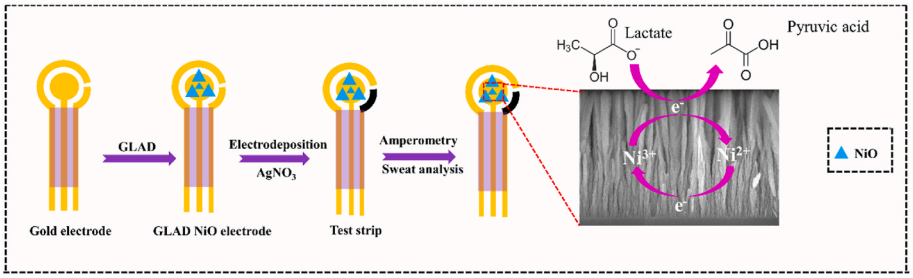

Scheme 1. Schematic representation for the fabrication of GLAD NiO on gold electrode for lactate detection.

including limited stability and high manufacturing cost. Furthermore, they are challenging to store and are sensitive to operation conditions, such as pH and temperature. Therefore, alternative approaches have emerged for the development of enzyme-free electrochemical sensors. Recently, the utilization of inorganic nanomaterials such as Zn (Zhao et al., 2015), Cu (Heo et al., 2021), Co (Chang et al., 2019), and Ni (Arivazhagan and Maduraiveeran, 2023; Kim et al., 2018; Miao et al., 2014), referred to as nanozymes, has garnered considerable attention due to their enzyme-like catalytic activity. These materials have been employed as novel catalysts for electrochemical signal amplification and constructing innovative electrochemical biosensors. Among the metal nanozyme sensors, nickel-based sensors possess the advantages of excellent catalytic properties, low toxicity, and economic feasibility. The high catalytic activity of Ni enables efficient and sensitive detection of target analytes, including lactate (Arivazhagan and Maduraiveeran, 2023; Kim et al., 2018; Miao et al., 2014).

Researchers have successfully fabricated Ni-based nanozyme lactate sensors through a diverse range of processes, including electrodeposition (Amin et al., 2019), chemical vapor deposition (Hutton et al., 2010), and physical vapor deposition (Chan et al., 2012). Here, we focus on the technique known as glancing angle deposition (GLAD) which is a physical vapor deposition process that involves depositing material onto a substrate oriented at oblique angles with respect to a vapor source, typically accompanied by substrate rotation (Abzieher et al., 2019; Yadav et al., 2022). This results in the formation of unique nanostructured thin films with columnar architectures, increasing the number of active sites available for catalysis with a high surface-to-volume ratio of the nanostructure. The increased surface area allows for a greater interaction between the analyte and catalyst, enhancing the sensitivity and lowering the detection limit of the sensor (Martin, 2009; Singer et al., 2020).

To our knowledge, there are no previous reports of GLAD NiO films in lactate detection. In this study, we fabricated GLAD NiO electrodes on planar gold surfaces prepared on flexible polyethylene terephthalate (PET) substrates, and we utilized these structures in the electrochemical determination of lactate. The GLAD NiO electrode offers a large surface area that dramatically increases the response to lactate, resulting in high sensitivity for lactate detection. The electrodes also show good selectivity and stability and were used to detect lactate in synthetic sweat samples. Preparation of GLAD films on flexible substrates also represents a relatively novel scenario, and our particular bio-sensing application, we expect the flexible substrates to be integrated into wearable devices more comfortably than conventional hard substrates (Xu et al., 2019; Yadav et al., 2022). The GLAD-NiO devices on PET were tested before and after tensile flexion, and they were found to have an excellent deformation tolerance.

2. Experimental section

2.1. Materials

Sodium L-lactate (~98%), L-ascorbic acid (≥99.0%), uric acid (≥99%), silver nitrate powder, and ammonium hydroxide were purchased from Sigma-Aldrich Canada. Potassium ferricyanide was purchased from Avantor JT Baker (USA). Sodium hydroxide (NaOH, ≥97.0%) was purchased from Fisher Scientific (Canada). Artificial eccrine perspiration was purchased from Pickering Laboratories, Inc. (USA). PET sheets were purchased from 3M Canada. Adhesive vinyl sheets were purchased from Digital Graphic Inc. (Canada). All aqueous solutions were prepared using highly purified water from a Millipore Milli-Q water system (≥18 MΩ cm). All chemicals were used without further purification.

2.2. Fabrication of nanocolumnar electrodes

Flexible gold electrodes were fabricated on PET by e-beam evaporation through a vinyl shadow mask. The vinyl mask was cut using a Graphtec CE7000 vinyl cutter to form 6 mm diameter circles as working electrodes and 1 mm wide strips as reference and counter electrodes. All were connected to 1.5 mm width lines to form the electrical contacts. These exposed areas were coated with 40 nm chromium as the adhesion layer and 200 nm Au using an Intlvac Nanochrome e-beam deposition system.

The GLAD NiO film was fabricated on the gold working electrodes using the following procedure. Kapton tape was cut to remove 6.5 mm circular openings, and these openings were aligned by hand to match the 6 mm diameter working electrodes patterned in the Cr/Au film. These masked substrates were then affixed to an aluminum chuck and loaded into a GLAD-enabled electron beam evaporation system (Kurt J. Lesker Company, USA). The system was equipped with computer-controlled stepper motors that enabled rotation and tilting of the substrate. For NiO deposition, NiO pellets (99.9%, Heeger Materials) were placed in graphite crucible liners, and the vacuum chamber was evacuated to a pressure less than 6×10^{-5} Pa. During deposition, the e-beam accelerating voltage was fixed at 7.5 kV while the e-beam position and current (~75 mA) were regularly adjusted to maintain an NiO deposition rate of approximately 0.35 nm s^{-1} and a deposition pressure of about 7×10^{-3} Pa. The substrates were oriented at a 74° angle with respect to the NiO vapor source and continuously rotated at a rate of one rotation per 10 nm of film growth. To facilitate scanning electron microscopy analysis (SEM, Hitachi S-4800, Japan), pieces of Si wafers were also fixed on the aluminum chuck and coated with NiO using the same GLAD processes, and following deposition, they were cleaved and mounted on aluminum stubs for analysis. The fabrication of proposed sensing platform and corresponding lactate oxidation is shown in Scheme 1.

2.3. Fabrication of solid-state Ag/AgCl reference electrodes

Solid-state Ag/AgCl reference electrodes were integrated with the patterned flexible electrodes using a fabrication approach closely mirroring our previous work (Wang et al., 2020). In brief, silver was electrochemically deposited on the designated gold reference electrode. This involved applying −0.1 V for 30 s to eliminate gas bubbles, followed by −0.5 V for 20 min in a solution of 0.1 M $AgNO_3$ and 1 M NH_4OH, using a commercial Ag/AgCl (1M KCl) electrode and a Pt wire as temporary reference and counter electrodes, respectively. The silver-coated

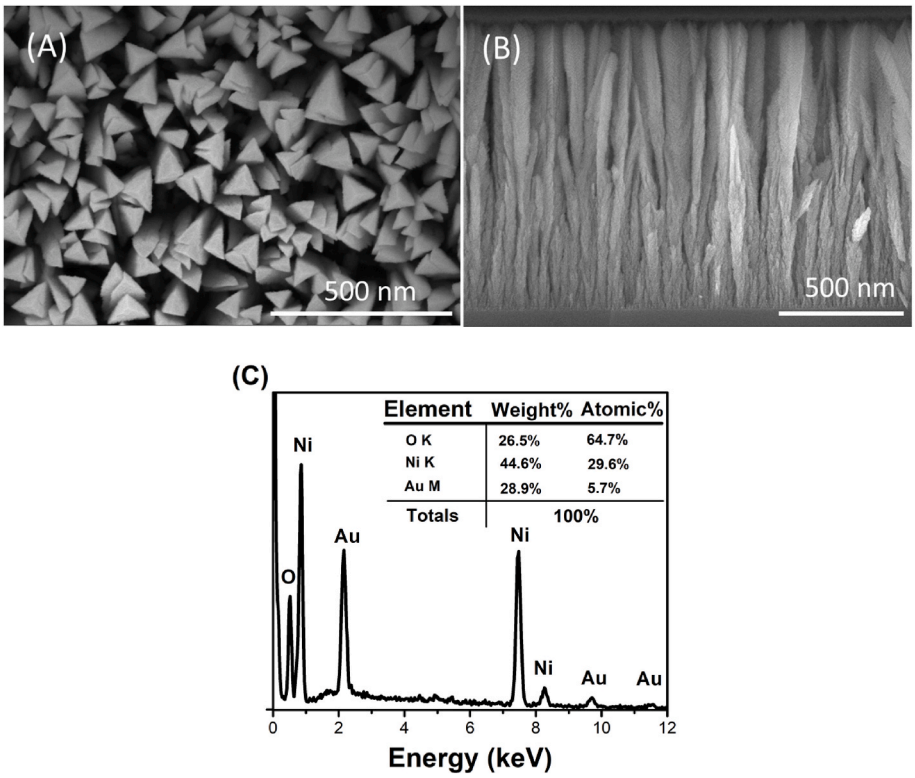

Fig. 1. Scanning electron microscopy (SEM) images depicting top view (A) and cross-sectional (B) views of the GLAD NiO thin film. (C) EDS data of GLAD NiO.

electrode was then treated with 6% bleach to produce Ag/AgCl. Afterward, it was rinsed in water to remove any loose AgCl and dried at room temperature. The reference electrode was then carefully immersed in 5% Nafion for 10 s and dried for 30 min. This step was repeated five times, after which the electrode was left to airdry overnight.

2.4. Electrochemical measurements

All electrochemical measurements were carried out using a 650A potentiostat from CH Instruments (Austin, Texas, USA) in a three-electrode configuration at room temperature. The working electrode was the GLAD NiO electrode with a 6 mm diameter, while the counter electrode was a coiled Pt wire. All potentials were referred to Ag/AgCl (1 M KCl). Prior to electrochemical measurements, all solutions were purged with N_2 for 30 min, and except for the optimization experiments, all electrochemical measurements were performed in 0.25 M NaOH. To ensure surface oxidation and stabilize the electrode response, the NiO electrodes underwent 30 cycles of cyclic voltammetry (CV) in the potential range of 0.0 to +0.7 V at 100 mV/s. After the activation process, the response of the GLAD NiO electrodes to lactate was evaluated by chronoamperometry (CA). All CA experiments, apart from the potential optimization, were conducted at an optimized potential of +0.55 V. After an initial stabilization period of 100 s, lactate was pipetted into the system at 100 s intervals while the solution was magnetically stirred at approximately 1200 rpm.

3. Results and discussion

3.1. Characterization of electrodes

Fig. 1 presents SEM images of a GLAD NiO film, revealing its microporous structure composed of closely packed yet separated vertically aligned columns. In the top view (Fig. 1A), a triangular columnar structure is observed, with an intercolumnar spacing of approximately 100 nm. The formation of these nanocolumns has been described in detail elsewhere, with the predominant growth mechanism being geometrical shadowing caused by the oblique angle of the substrate promoting the formation of distinct columns (Amassian et al., 2007; Barranco et al., 2016; Martin, 2009). Previous studies have shown that metal oxide GLAD electrodes have 30–40% void spaces and their catalytic properties are superior to compact thin films (Garcia-Garcia et al., 2016; Singer et al., 2020; Tripathi et al., 2022). In the side-view (Fig. 1B), columnar structures with increasing diameter from base to tip are observed, accompanied by a reduction in number density. As can be seen in Fig. 1C, energy dispersive x-ray spectroscopy (EDS) spectra reveal strong peaks corresponding to Ni and O with atomic fractions of 29.6% and 64.7%, respectively. These data suggest a nickel oxide composition other than NiO, possibly an $Ni(OH)_2$ surface layer spontaneously formed via interactions with atmospheric water vapor. The small fraction of Au (5.7%) is derived from the underlying gold electrodes.

Electrochemical impedance spectroscopy (EIS) is a robust technique for detecting surface phenomena, including charge transfer impedance and capacitance. Fig. S1 showcases the Nyquist plots derived from the EIS measurements of the fabricated electrodes. Upon fitting these to the standard Randles equivalent circuit (Lisdat and Schafer, 2008), both the GLAD NiO and bare gold electrodes exhibit a charge transfer resistance of roughly 300 Ω, however the capacitance of the GLAD NiO structure (5.4 μF) is larger than the bare gold electrode (4.6 μF). This variation might be linked to the change in dielectric constant, the possible involvement of Ni^{2+}/Ni^{3+} in the charge transfer mechanism, or geometrical changes in the electrode's double layer due to the high surface area of the GLAD structure (Lazanas and Prodromidis, 2023). In any case, the high surface-area-to-geometrical-area ratio of the GLAD NiO electrodes is known to create a high concentration of active sites for reactions, enhancing the rates of processes such as adsorption, catalysis, and charge transfer (Garcia-Garcia et al., 2016).

The series of Ni reactions relevant to lactate detection are shown below:

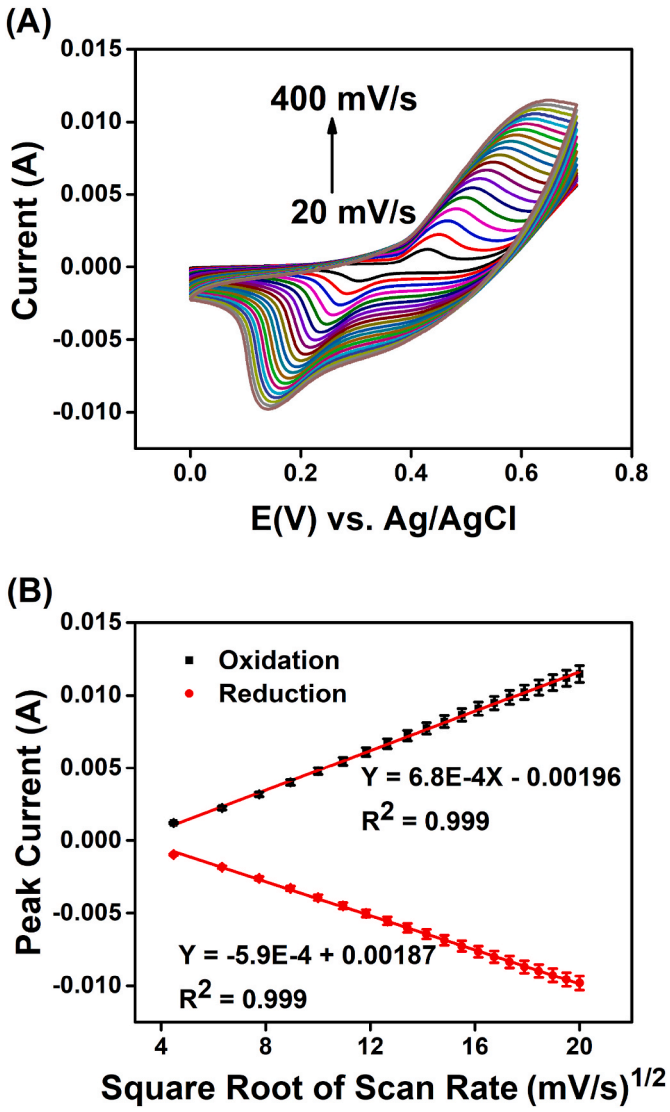

Fig. 2. Different scan rates for GLAD NiO electrodes in 0.25 M NaOH containing 1 mM lactate. (A) Cyclic voltammograms at varying scan rates from 20 to 400 mV/s, and (B) the corresponding relationships between anodic/cathodic peak currents and square root of scan rate.

$$NiO + H_2O \Rightarrow Ni(OH)_2 \quad (1)$$

$$Ni(OH)_2 + OH^- \rightleftharpoons NiOOH + H_2O + e^- \quad (2)$$

$$NiOOH + \text{lactate} \Rightarrow Ni(OH)_2 + \text{pyruvic acid} \quad (3)$$

Eq. (1) is spontaneous in an aqueous environment. The NiOOH, which is well-known as an efficient electrocatalyst for oxidation of lactate, is generated from $Ni(OH)_2$ via Eq. (2) under basic conditions. This species is then reduced to $Ni(OH)_2$ during lactate oxidation in Eq. (3), but it is regenerated by Eq. (2) to complete the catalytic cycle (Miao et al., 2014; Kim et al., 2018). We and others (Singer et al., 2020) have noted that the initial $Ni^{2+/3+}$ redox peak currents generated via (2) tend to increase as multiple cycles of cyclic voltammetry are performed in NaOH, and they stabilize after a number of cycles (Fig. S2). We thus term this pre-cycling process "activation" and note that GLAD NiO electrodes must be activated to maximize the surface concentration of the catalytic Ni^{3+}. This is achieved by performing CV of the GLAD NiO electrode in a 0.25 M NaOH solution within a voltage range of 0.0 V–0.7 V vs Ag/AgCl (1M KCl) until stable and reproducible $Ni^{2+/3+}$ peaks are observed (Fig. S2). From the figure, it is evident that as the number of cycles increases, the anodic and cathodic peak positions gradually shift to more positive and negative potentials, respectively, which can be attributed to the continuous enrichment of the NiOOH layer on the electrodes in the highly concentrated alkaline solution until it reaches saturation thickness (Lazanas and Prodromidis, 2023). From the anodic peak area of the saturated CV, the surface coverage ($\Gamma = Q/nFA$, where Q is the integrated charge, n is the number of electrons, F is Faraday's constant and A is the geometrical area of the electrode) of $Ni(OH)_2$ on GLAD NiO electrodes was calculated to be $4.3(\pm 0.4) \times 10^{-7}$ mol cm^{-2}, which is similar to what has been reported for NiO films deposited at oblique angles (Garcia-Garcia et al., 2016).

3.2. Electrochemical detection of lactate

After surface activation of the GLAD NiO electrodes, their performance towards electrochemical detection of lactate was evaluated. Fig. S3 shows CV responses of a GLAD NiO electrode in the absence and presence of 1 mM lactate. From the voltammograms, it is obvious that the $Ni^{2+/3+}$ peak intensity increases in the presence of lactate, indicating the oxidation of lactate by the electrode. The increase in the peak potential separation ($\Delta E_p = E_{pa} - E_{pc}$) for the redox pair in the presence of lactate is attributed to restricted diffusion into the nanocolumnar architecture (Garcia-Garcia et al., 2016; Kim et al., 2018).

To gain a deeper understanding of the electrocatalytic properties of the GLAD NiO electrodes, different potential scan rates (20–400 mV/s) were used while maintaining a fixed (1 mM) lactate concentration in 0.25 M NaOH solution. Fig. 2a displays the resulting voltammograms. Based on the figure, it is evident that the ratios of the anodic peak currents to the cathodic peak currents are greater than 1 (~1.2) for all scan rates, implying an irreversible lactate oxidation and the excellent electrocatalytic properties of the GLAD NiO electrode. The increase in the peak potential for lactate oxidation with increasing scan rate suggests restrictions imposed on the diffusion of lactate into the GLAD NiO electrode and/or adsorption of lactate or its oxidation product (pyruvic acid) on the electrode surface. A plot of anodic peak current vs. the square root of the scan rate, Fig. 2B, yielded a straight line ($R^2 = 0.999$), indicating that the electrocatalytic oxidation of lactate on GLAD NiO is primarily governed by the diffusion of lactate molecules at the interface between electrodes and electrolyte.

Before delving into the investigation of the sensing capabilities of the GLAD NiO electrodes, it is essential to determine the optimal applied potential and solution pH (i.e. concentration of NaOH) for which the lactate oxidation current reaches its maximum value. Fig. S4 illustrates the electrode response to variations in applied potential while maintaining fixed concentrations of 0.25 M NaOH and 1 mM lactate. The lactate oxidation current exhibits a continuous increase with increasing potential until it reaches 0.55 V vs Ag/AgCl (1M KCl.), which is identified as the optimum value. To optimize the pH of the solution, the applied electrode potential was set at 0.55 V and the concentration of NaOH varied. Fig. S5 shows that increasing the NaOH concentration (0.05 M–0.25 M) generates increasingly higher lactate oxidation current. Previous reports using GLAD NiO electrodes have shown that increasing the NaOH concentration beyond 0.25 M increases the background current and compromises the overall stability and performance of the sensor (Singer et al., 2020; Tripathi et al., 2022), and thus 0.25 M NaOH was chosen as the optimum and used for all subsequent measurements.

To investigate the lactate oxidation rate by the catalytic GLAD NiO electrodes, CA measurements of an electrode in 1 mM lactate were conducted using the optimized conditions established above. As shown in Fig. S6, the oxidation current is dominated by the rate of the electrocatalytic reaction. The relationship between the catalytic current (I_{CAT}) in the presence of lactate and the background current (I_B) in the absence of lactate is proportional to the square root of time, and can be written as (Niu et al., 2013; Singer et al., 2020): $\frac{I_{CAT}}{I_B} = (\pi \kappa_{CAT} C_0 t)^{1/2}$, where κ_{CAT} is the catalytic rate constant, C_0 the bulk concentration of lactate, and t the elapsed time. From the slope of the I_{cat}/I_B curve

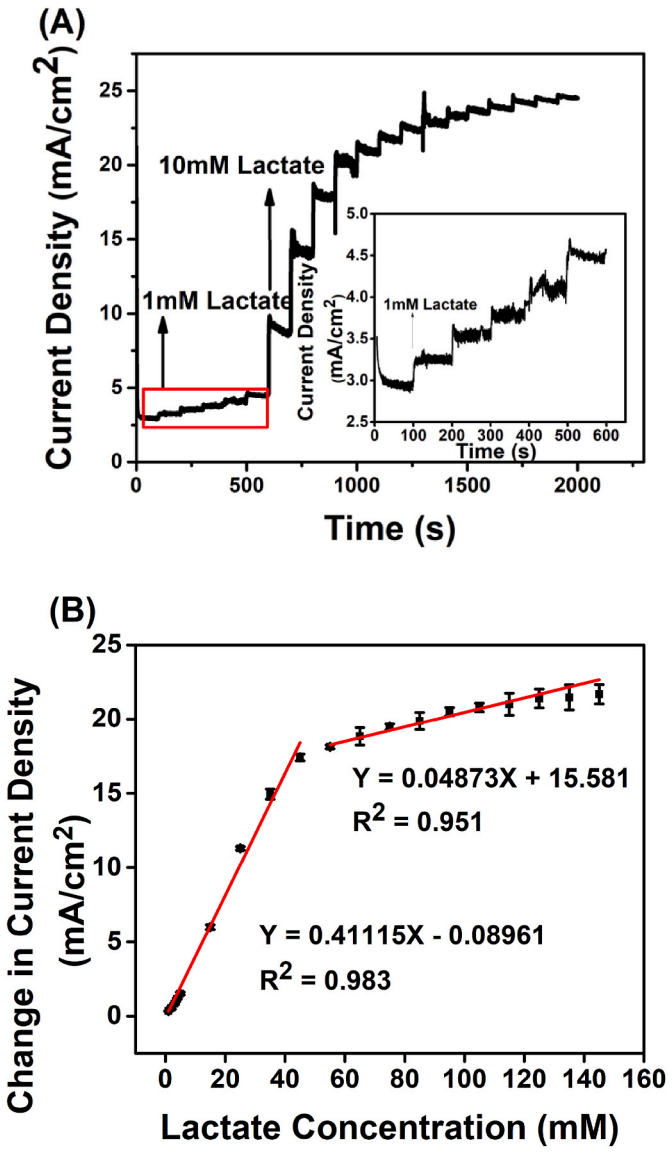

Fig. 3. (A) Chronoamperometric responses of the GLAD-NiO lactate sensor to successive additions of 1 mM and 10 mM lactate at the optimum applied potential (0.55 V) and NaOH concentration (0.25 M). Inset: Zoomed-in view of the region inside the red box corresponding to CA responses in the low concentration range (<5 mM). (B) The change in current density of the GLAD NiO lactate sensor to different lactate concentrations from 1 mM to 145 mM. (For interpretation of the references to colour in this figure legend, the reader is referred to the Web version of this article.)

(Fig. S6B), a κ_{CAT} value of 95 M^{-1} s^{-1} is calculated for the electrode.

The Michaelis–Menten constant (K_M^{APP}) reflect the affinity between an enzyme and its substrate. It represents the substrate concentration at which the enzyme achieves half of its maximum catalytic activity. As GLAD NiO acts as a nanozyme, the K_M^{APP} can be calculated from the Lineweaver–Burk equation (Zhao et al., 2015): $\frac{1}{i} = \frac{K_M^{APP}}{iMax}\frac{1}{C} + \frac{1}{iMax}$, Where the i and i_{Max} represent the response current, maximum current respectively, and C is the concentration of lactate. The GLAD NiO exhibits a Michaelis–Menten constant of 164 mM.

Table 1
Comparison of the performance of the GLAD NiO electrode with contemporary reports of nonenzymatic lactate sensors.

Materials	Linear range	Limit of detection	Sensitivity	Ref.
NiO and Ni $(OH)_2$	7.76–32.76 mM	530 and 590 μM	9.08 and 35.7 μA $mM^{-1}cm^{-2}$	Kim et al. (2018)
NiO NPs/ GCE	0.005–5 mM	5.7 μM	–	Amin et al. (2019)
NiCoLDH	2–26 mM	399 μM	83.98 μA $mM^{-1}cm^{-2}$	Wang et al. (2022)
NiF/ $NiCo_2O_4$	5–50 mM	–	430 μA $mM^{-1}cm^{-2}$	Elakkiya and Maduraiveeran (2019)
NiO, NiO250, NiO350, and NiO450	Up to 25 mM	95, 27, 42, and 72 μM	3.30, 62.35, 38.88, and 9.50 μA $mM^{-1}cm^{-2}$	Kim et al. (2019)
Pt/Ni-MOF	0.01–0.9 and 1–4 mM	5 μM	106.61 and 29.53 μA mM^{-1}	Manivel et al. (2018)
GLAD NiO	1–45 mM	3 μM	412 μA $mM^{-1}cm^{-2}$	This work

3.3. Selectivity of the sensor and the detection of lactate in sweat samples

Selectivity plays a crucial role in the functionality of a sensor. In the context of lactate detection in sweat samples, the presence of interferents such as uric acid (UA), ascorbic acid (AA), and glucose (Glu) poses significant challenges (Kim et al., 2019; Manivel et al., 2018). Existing reports indicate that the concentrations of these interfering compounds in sweat typically peak around 0.1 mM, while the lactate concentration far surpasses these interferents, reaching average concentrations of approximately 43 mM during endurance exercise (Anastasova et al., 2017; Derbyshire et al., 2012). To evaluate the selectivity of GLAD NiO electrodes for lactate detection, CA experiments were performed by individually introducing 0.25 mM Glu, 0.1 mM AA, and 0.1 mM UA into a solution containing 3 mM lactate. Fig. 4A illustrates that the oxidation currents arising from the interferents are negligible compared to the response generated by lactate. Although there is a slight response (<18%) to Glu and AA, the signal for lactate remains sufficiently discernible in the presence of these potential interferents.

Fig. 3 shows the CA response of the GLAD NiO electrode to successive additions of a broad range of lactate concentrations (1 mM–145 mM) under the optimized potential and NaOH concentration conditions. With each addition of lactate, the electrode responded rapidly reaching 95% of the steady-state current within ~5 s. A plot of change in current density as a function of lactate concentration (Fig. 3B) yields two linear responses with distinct slopes in the 0–45 mM (slope = 0.41 mA/cm^2·mM, R^2 = 0.983) and 50–145 mM (slope = 0.05 mA/cm^2·mM, R^2 = 0.951) ranges. Each data point symbolizes an average of three independent measurements, with error bars showing the standard deviation of the measurements. The small slope in the high concentration range indicates the sensor's response is approaching saturation for lactate concentrations greater than 45 mM which corresponds to the maximum concentration typically found in human sweat (Anastasova et al., 2017; Derbyshire et al., 2012). The GLAD NiO electrodes demonstrate a high sensitivity of 410 μA mM^{-1} cm^{-2}, which is higher than most recently reported values for Ni-based lactate electrochemical sensors (see Table 1). The high sensitivity of the GLAD NiO electrode is ascribed to the large surface area created by the GLAD structure and the associated high electrocatalytic lactate oxidation rate at the electrode. The theoretical limit of detection (LOD) of the sensor was calculated to be 3 μM lactate, calculated as 3σ/slope (σ is the standard deviation for the lowest concentration in the calibration plot). This value represents the lowest LOD ever reported for NiO-based nonenzymatic electrochemical lactate detection. Table 1 shows a comparison of the performance parameters

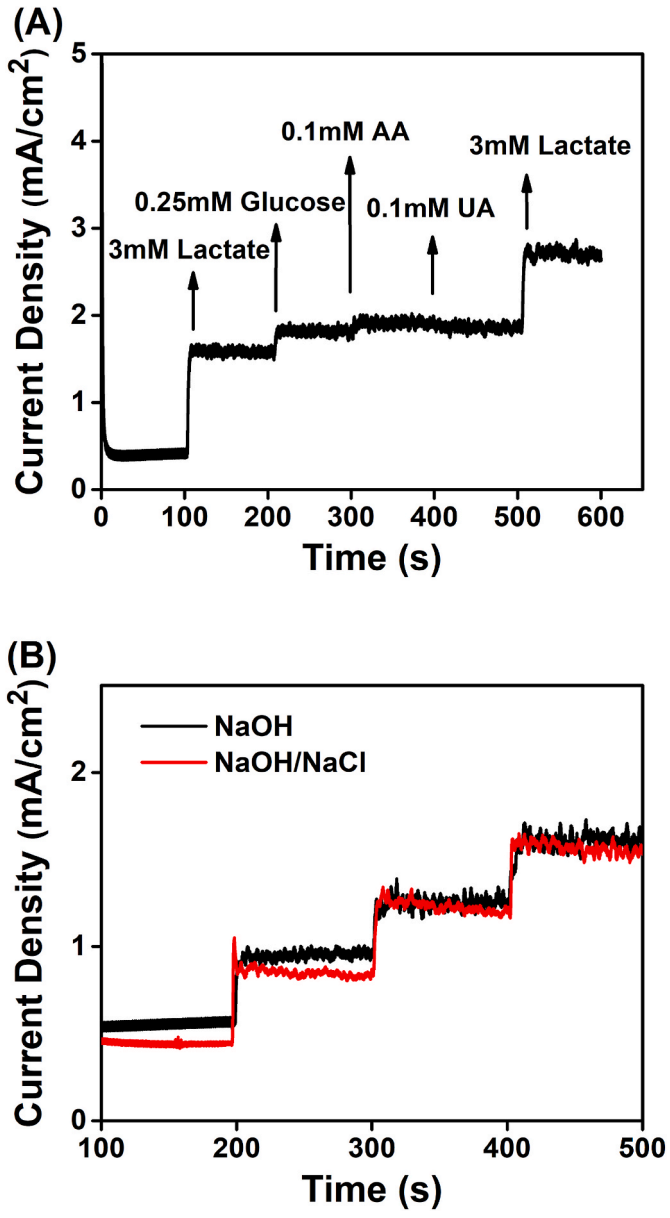

Fig. 4. (A) Chronoamperometric responses of the lactate sensor to 3 mM lactate, 0.25 mM glucose, 0.1 mM ascorbic acid, and 0.1 mM uric acid. (B) Chronoamperometric response to additions of 1 mM lactate in two different matrices: 0.25 M NaOH (black), 0.25 M NaOH and 0.25 M NaCl (red), A constant potential (0.55V) was applied between the working and counter electrodes. (For interpretation of the references to colour in this figure legend, the reader is referred to the Web version of this article.)

for nonenzymatic sensors used for lactate detection.

It is well-known that, apart from high lactate concentration, sweat also contains significantly elevated levels of chloride ions, which can have a negative impact on the sensitivity of the sensor (Singer et al., 2020). To assess the influence of chloride ions on the sensor's performance, CA experiments were conducted using 0.25 M NaOH and a solution consisting of 0.25 M NaOH and 0.25 M NaCl. Fig. 4B illustrates the results obtained when we introduce three separate additions of 1 mM lactate to these two electrolytic solutions. No discernible differences in response currents are observed between the two solutions, suggesting that the GLAD NiO electrodes are resistant to chloride poisoning, effectively mitigating the potential interference caused by high chloride ion concentrations found in human sweat.

To demonstrate the GLAD NiO electrode's applicability in the

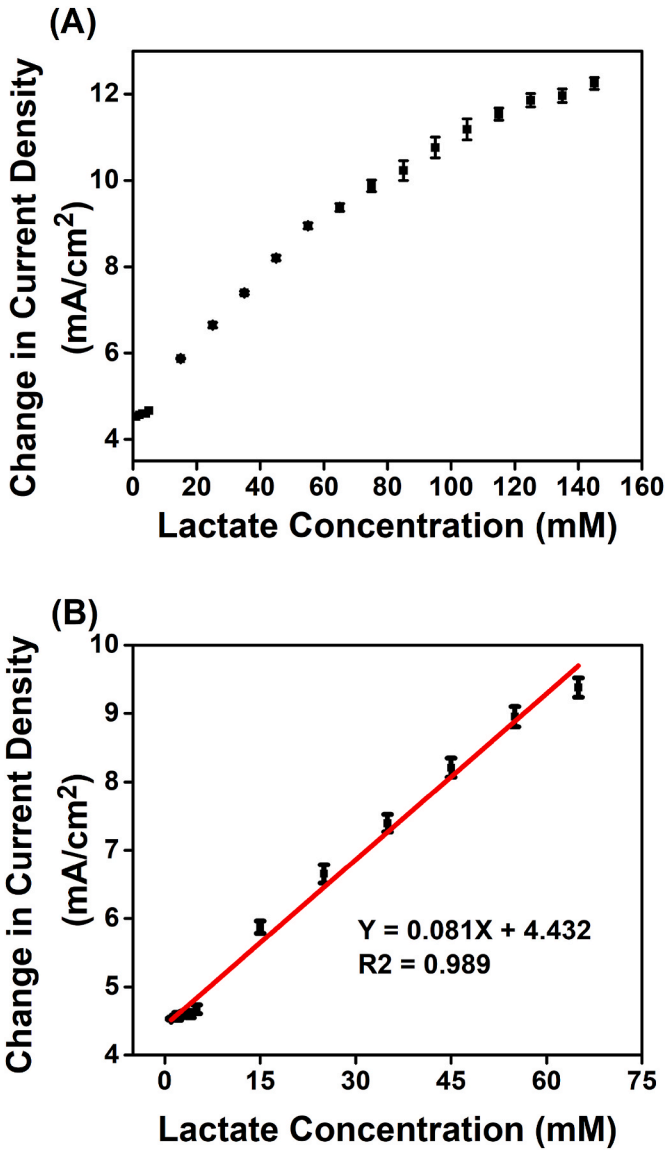

Fig. 5. (A) Chronoamperometric response of the sensor (held at a constant applied potential of 0.55 V in 1:1 v/v artificial sweat and 0.25 M NaOH) to successive additions of 1 mM and 10 mM lactate. (B) Linear fitting curve for the responses of the GLAD NiO-based biosensor to various lactate concentrations. Data points are averages of three independent electrode measurements with small error bars.

determination of lactate in sweat samples, an artificial sweat (with composition given in Table S1) was used. CA experiments were conducted using a 1:1 v/v ratio of the artificial sweat and a 0.5 M NaOH solution spiked with varying concentrations of lactate. Fig. 5A illustrates the response of the GLAD NiO electrodes to successive additions of lactate ranging from 1 mM up to 145 mM. Although the overall sensitivity (across the entire concentration range) of the sensor is reduced

Table 2
The determination of lactate in sweat by GLAD NiO electrode using a standard addition method (n = 3).

Sample concentration (mM)	Spiked sample concentration (mM)	Measured concentration (mM)	Recovery (%) ± RSD
2.00	1.00	2.82	98 ± 5
2.00	3.00	4.59	86 ± 6
2.00	5.00	6.20	88 ± 5

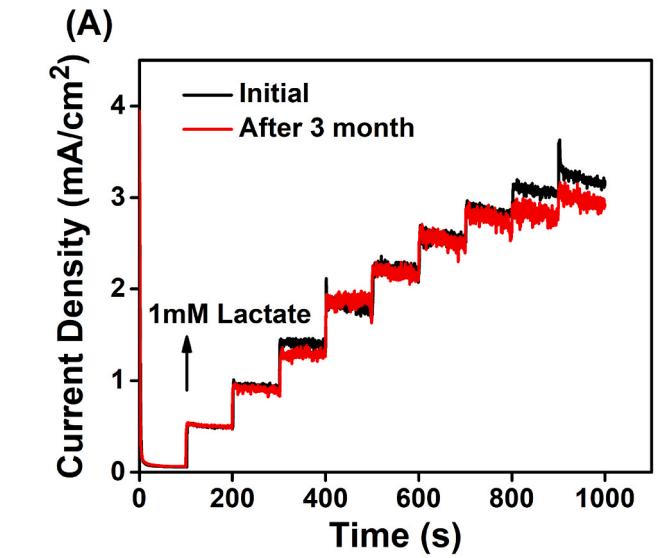

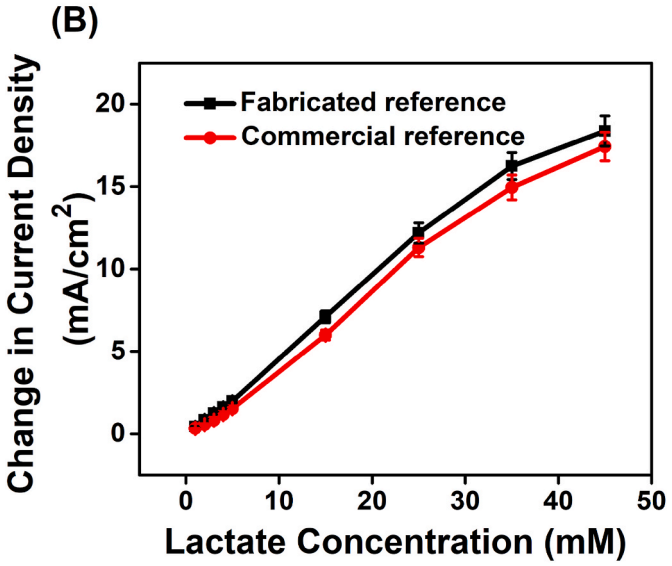

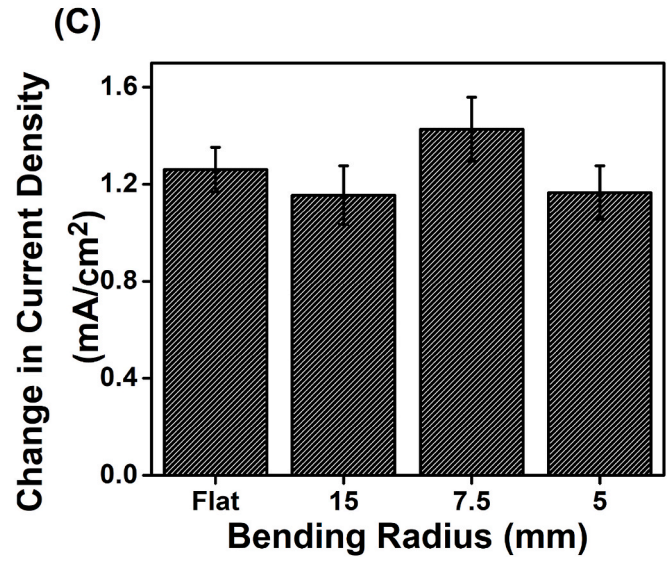

(caption on next column)

Fig. 6. Storage stability of the GLAD NiO electrodes for the detection of lactate (1 mM lactate) in 0.25 M NaOH at the optimum applied potential of 0.55 V. (B) Chronoamperometric responses of the sensor using commercial reference electrode (red line, with 0.55 V CA potential) and fabricated reference electrode (black line, with 0.35 V CA potential) to successive additions of 1 mM and 10 mM lactate in 0.25 M NaOH. Data points are averages of three independent electrode measurements with small error bars. (C) Change in current density in response to addition of 3 mM lactate for the GLAD NiO electrodes after different degrees of bending. (For interpretation of the references to colour in this figure legend, the reader is referred to the Web version of this article.)

(slope of 80 μA/cm^2·mM in sweat vs. 410 μA/cm^2·mM in NaOH solution, Fig. 3B), the response demonstrates an excellent linear relationship in the clinically relevant lactate concentration range from 1 mM to 65 mM (Fig. 5B), with a LOD of 16 μM, which is less than the concentrations typically found in sweat (Niu et al., 2013). To check the practical utility of the developed sensor, the recovery study at three different concentrations was performed and recovery values were calculated based on difference between added value and measured value as shown in Table 2. It is found that the recoveries values ranged from 86 to 98% and corresponding RSDs vary from 5 to 6% which shows that the developed sensor is suitable for detection of lactate in complex matrix.

Fig. 6A compares the performance of the GLAD NiO electrode immediately after preparation to performance after 3 months of storage in dry ambient conditions in a laboratory drawer. There was no significant difference in the measured lactate oxidation currents, indicating the sensor is stable and not prone to losing sensitivity for lactate detection under storage conditions.

In an effort to gather evidence supporting the feasibility of GLAD-based devices as commercial test strips for point-of-care applications, we also fabricated devices with on-chip reference and auxiliary electrodes using the methods described in the experimental section. An on-chip reference (rather than an external liquid-based electrode) is clearly advantageous for a convenient, real-world implementation. Comparing the behavior of the device with on-chip reference electrode against a commercial (Ag/AgCl) reference electrode, a potential shift was observed, as illustrated in Fig. S7, which was attributed to the large variation in Cl^- concentration between the commercial and solid references. This shift resulted in the alteration of the oxidation potential for lactate oxidation to 0.35 V. Applying the much lower potential of 0.35 V vs. the in-house fabricated Ag/AgCl electrode in a CA experiment for the oxidation of lactate, Fig. 6B shows that the GLAD NiO response is linear in the concentration range of 1–45 mM, with sensitivity (slope) equivalent to that obtained earlier with the commercial reference electrode (i.e., Fig. 3).

Flexibility is of paramount importance for wearable sensors. Fig. 6C presents the stability of the electrodes under tensile flexural strain at various bending radii. The electrodes were bent at each radius for 5 min, then returned to their original state for CA testing. The limited variation in the current density for 3 mM lactate, as shown in Fig. 6C, indicates the potential of our electrodes for use in future wearable sensor applications.

4. Conclusion

In summary, a nanostructured GLAD NiO film on a gold substrate was fabricated for lactate detection. The GLAD NiO electrodes exhibited a sensitive response for lactate detection (412 μA mM^{-1} cm^{-2}), with a limit of detection (3 μM) well below typical lactate concentrations in human sweat. The high performance of the nanostructured thin films is attributed to their excellent electrocatalytic activity and high specific surface area. Despite the influence of the matrix in the sweat sample, the sensor exhibits a linear range of 1 mM–65 mM for lactate detection, covering the lactate concentration found in sweat. Additionally, no poisoning effects are observed from exposure to high concentrations of chloride ions, and selective detection of lactate was maintained in the

presence of interfering species. Even after 3 months of dry storage under ambient conditions, our sensor maintained its performance in detecting lactate, with no significant change in the lactate oxidation current response. The proposed nanozyme sensor utilizing GLAD NiO electrodes offers selective and reliable lactate detection, making it a promising practical device for lactate monitoring. The results of this study provide not only new prospects for the development of more sensitive and stable electrochemical sensors, but also provide a basis for developing unique and robust biochemical detection methods. The GLAD NiO, when implemented in a test strip format, exhibits performance comparable to a standard three-electrode system and demonstrated excellent flexibility and stable performance after bending across various bending radii, and offers a range of advantages, from improved sensitivity to real-time monitoring and wearability, making it well suited for point-of-care testing.

CRediT authorship contribution statement

Pei Li: Writing – original draft, Visualization, Validation, Software, Methodology, Formal analysis, Data curation, Conceptualization. **Pramod K. Kalambate:** Writing – review & editing, Visualization, Methodology, Formal analysis, Data curation. **Kenneth D. Harris:** Writing – review & editing, Supervision, Resources, Project administration, Methodology, Investigation, Funding acquisition, Formal analysis, Data curation. **Abebaw B. Jemere:** Writing – review & editing, Visualization, Supervision, Resources, Project administration, Investigation, Funding acquisition, Formal analysis, Data curation, Conceptualization. **Xiaowu (Shirley) Tang:** Writing – review & editing, Validation, Supervision, Resources, Project administration, Investigation, Funding acquisition, Formal analysis, Data curation, Conceptualization.

Declaration of competing interest

The authors declare that they have no known competing financial interests or personal relationships that could have appeared to influence the work reported in this paper.

Data availability

Data will be made available on request.

Acknowledgements

The authors acknowledge Paul Concepcion for SEM imaging. This work is supported jointly by the Waterloo Institute for Nanotechnology and the National Research Council of Canada.

Appendix A. Supplementary data

Supplementary data to this article can be found online at https://doi.org/10.1016/j.biosx.2024.100455.

References

Abzieher, T., Moghadamzadeh, S., Schackmar, F., Eggers, H., Sutterlüti, F., Farooq, A., Kojda, D., Habicht, K., Schmager, R., Mertens, A., Azmi, R., Klohr, L., Schwenzer, J. A., Hetterich, M., Lemmer, U., Richards, B.S., Powalla, M., Paetzold, U.W., 2019. Adv. Energy Mater. 9 (12), 1802995–1803008.
Amassian, A., Kaminska, K., Suzuki, M., Martinu, L., Robbie, K., 2007. Appl. Phys. Lett. 91 (17), 173114–173118.
Amin, S., Tahira, A., Solangi, A., Mazzaro, R., Ibupoto, Z.H., Vomiero, A., 2019. Anal. Methods 11 (28), 3578–3583.
Anastasova, S., Crewther, B., Bembnowicz, P., Curto, V., Ip, H.M., Rosa, B., Yang, G.Z., 2017. Biosens. Bioelectron. 93, 139–145.
Arivazhagan, M., Maduraiveeran, G., 2023. Mater. Chem. Phys. 295, 127084–127095.
Baranwal, J., Barse, B., Gatto, G., Broncova, G., Kumar, A., 2022. Chemosensors 10 (9), 363–385.
Barranco, A., Borras, A., Gonzalez-Elipe, A.R., Palmero, A., 2016. Prog. Mater. Sci. 76, 59–153.
Chan, K.T., Kan, J.J., Doran, C., Ouyang, L., Smith, D.J., Fullerton, E.E., 2012. Philos. Mag. A 92 (17), 2173–2186.
Chang, A.S., Memon, N.N., Amin, S., Chang, F., Aftab, U., Abro, M.I., dad Chandio, A., Shah, A.A., Ibupoto, M.H., Ansari, M.A., Ibupoto, Z.H., 2019. Electroanalysis 31 (7), 1296–1303.
Chuang, C.K., Wang, T.J., Yeung, C.Y., Lin, D.S., Lin, H.Y., Liu, H.L., Ho, H.T., Hsieh, W. S., Lin, S.P., 2009. J. Chromatogr., A 1216 (51), 8947–8952.
Derbyshire, P.J., Barr, H., Davis, F., Higson, S.P., 2012. J. Physiol. Sci. 62 (6), 429–440.
Elakkiya, R., Maduraiveeran, G., 2019. New J. Chem. 43 (37), 14756–14762.
Garcia-Garcia, F.J., Salazar, P., Yubero, F., González-Elipe, A.R., 2016. Electrochim. Acta 201, 38–44.
Heo, S.G., Yang, W.S., Kim, S.J., Park, Y.M., Park, K.T., Oh, S.J., Seo, S.J., 2021. Appl. Surf. Sci. 555, 149638–149644.
Hutton, L.A., Vidotti, M., Patel, A.N., Newton, M.E., Unwin, P.R., Macpherson, J.V., 2010. J. Phys. Chem. C 115 (5), 1649–1658.
Kim, S.J., Kim, K.J., Kim, H.J., Lee, H.N., Park, T.J., Park, Y.M., 2018. Electrochim. Acta 276, 240–246.
Kim, S.J., Yang, W.S., Kim, H.J., Lee, H.N., Park, T.J., Seo, S.J., Park, Y.M., 2019. Ceram. Int. 45 (17), 23370–23376.
Kruse, J.A., Zaidi, S.A., Carlson, R.W., 1987. Am. J. Med. 83 (1), 77–82.
Lazanas, A.C., Prodromidis, M.I., 2023. ACS Meas. Sci. Au 3 (3), 162–193.
Lisdat, F., Schafer, D., 2008. Anal. Bioanal. Chem. 391 (5), 1555–1567.
Manivel, P., Suryanarayanan, V., Nesakumar, N., Velayutham, D., Madasamy, K., Kathiresan, M., Kulandaisamy, A.J., Rayappan, J.B.B., 2018. New J. Chem. 42 (14), 11839–11846.
Martin, P.M., 2009. Handbook of Deposition Technologies for Films and Coatings: Science, Applications and Technology, third ed. William Andrew.
Md Shakhih, M.F., Rosslan, A.S., Noor, A.M., Ramanathan, S., Lazim, A.M., Wahab, A.A., 2021. J. Electrochem. Soc. 168 (6), 67502–67517.
Messonnier, L.A., Emhoff, C.A., Fattor, J.A., Horning, M.A., Carlson, T.J., Brooks, G.A., 2013. J. Appl. Physiol. 114 (11), 1593–1602.
Miao, Y., Ouyang, L., Zhou, S., Xu, L., Yang, Z., Xiao, M., Ouyang, R., 2014. Biosens. Bioelectron. 53, 428–439.
Niu, X., Lan, M., Zhao, H., Chen, C., 2013. Anal. Chem. 85 (7), 3561–3569.
Rassaei, L., Olthuis, W., Tsujimura, S., Sudholter, E.J., van den Berg, A., 2014. Anal. Bioanal. Chem. 406 (1), 123–137.
Rattu, G., Khansili, N., Maurya, V.K., Krishna, P.M., 2020. Environ. Chem. Lett. 19 (2), 1135–1152.
Rimachi, R., De Carvahlo, F.B., Orellano-Jimenez, C., Cotton, F., Vincent, J.L., De Backer, D., 2012. Anaesth. Intensive Care 40 (3), 427–432.
Ronkainen, N.J., Halsall, H.B., Heineman, W.R., 2010. Chem. Soc. Rev. 39 (5), 1747–1763.
Singer, N., Pillai, R.G., Johnson, A.I.D., Harris, K.D., Jemere, A.B., 2020. Mikrochim. Acta 187 (4), 196–206.
Tripathi, A., Elias, A.L., Jemere, A.B., Harris, K.D., 2022. ACS Food Sci. Technol. 2 (8), 1307–1317.
Wang, Y., Ausri, I.R., Wang, Z., Derry, C., Tang, X.S., 2020. Sensor. Actuator. B Chem. 308, 127645–127653.
Wang, Y.X., Tsao, P.K., Rinawati, M., Chen, K.J., Chen, K.Y., Chang, C.Y., Yeh, M.H., 2022. J. Chem. Eng. 427, 131687–131696.
Xu, M., Obodo, D., Yadavalli, V.K., 2019. Biosens. Bioelectron. 124–125, 96–114.
Yadav, S., Senapati, S., Kumar, S., Gahlaut, S.K., Singh, J.P., 2022. Biosensors 12 (12), 1115–1157.
Zhao, Y., Fang, X., Gu, Y., Yan, X., Kang, Z., Zheng, X., Lin, P., Zhao, L., Zhang, Y., 2015. Colloids Surf., B 126, 476–480.